JCTC Journal of Chemical Theory and Computation

Article

pubs.acs.org/JCTC

Quasiclassical Trajectory Studies of the Photodissociation Dynamics of NO_3 from the D_0 and D_1 Potential Energy Surfaces

Bina Fu,*[,†,‡] Joel M. Bowman,[†] Hongyan Xiao,[§] Satoshi Maeda,[∥] and Keiji Morokuma[†,§]

[†]Department of Chemistry and Cherry L. Emerson Center for Scientific Computation, Emory University, Atlanta, Georgia 30322, United States

[‡]State Key Laboratory of Molecular Reaction Dynamics and Center for Theoretical and Computational Chemistry, Dalian Institute of Chemical Physics, Chinese Academy of Sciences, Dalian 116023, People's Republic of China

[§]Fukui Institute for Fundamental Chemistry, Kyoto University, Kyoto 606-8103, Japan

[∥]Department of Chemistry, Faculty of Science, Hokkaido University, Sapporo 060-0810, Japan

Supporting Information

ABSTRACT: We report new global potential energy surfaces (PESs) for the D_0 and D_1 states of NO_3. The PESs are permutationally invariant fits to roughly 90 000 electronic energies (MS-CAS(17e,13o)PT2/aug-cc-pVTZ). Hundreds of thousands of quasiclassical trajectories are run from the D_0 global minimum and one previously identified "roaming saddle point" as well as a roaming saddle point on D_1, identified previously [Xiao, H.; Maeda, S.; Morokuma, K. *J. Chem. Theory Comput.* **2012**, *8*, 2600]. The calculations are done at a total energy of relevance to recent experiments where, together with theoretical analysis [Grubb, M. P.; Warter, M. L.; Xiao, H.; Maeda, S.; Morokuma, K.; North, S. W. *Science* **2012**, *335*, 1075], point to roaming pathways to the O_2+NO products on both D_1 and D_0. Detailed comparisons with experiment are made for the distributions of O_2 vibrational and rotational states, the relative translational energy and the NO rotational states, and the NO **v**-**j** vector correlation.

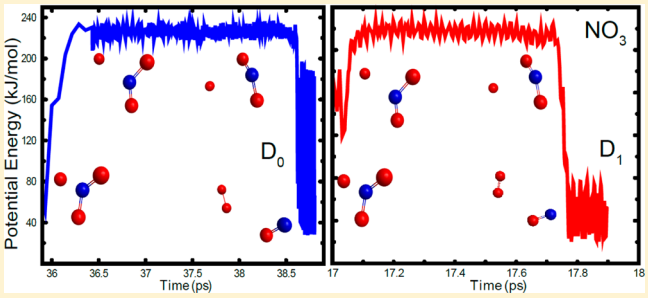

1. INTRODUCTION

Roaming, as a recently verified unusual pathway to molecular products from unimolecular dissociation, has received considerable attention both theoretically and experimentally.[1−3] In 2004, in a joint experimental and theoretical report, the term "roaming" was coined to describe a second pathway for the H_2+CO molecular channel in the photodissociation of H_2CO.[4] In brief, this pathway can be described as a self-reaction of incipient radicals, in the case of H_2CO, these are H and HCO, and the molecular products are H_2 and CO. After the first discovery of the roaming mechanism in the photodissociation of H_2CO, evidence of roaming has been observed in several other molecular[5−9] and even radical[10,11] dissociation systems.

Most of the studies of roaming dynamics are discussed for reactions on the ground electronic state. Very recently, North and co-workers, presented evidence of two distinct pathways for the formation of NO+O_2 in the photolysis of the nitrate radical (NO_3) at 588 nm.[12,13] The dominant pathway is characterized by vibrationally excited O_2 (v = 5−10) and rotationally cold NO; while the second one is vibrationally colder O_2 (v = 0−4) and rotationally hotter NO. In the initial experimental reports of the bimodal O_2 vibrational distribution, a roaming mechanism was proposed to explain the vibrationally hot component of the distribution.[12,13] The proposal was based on a similar bimodal distribution in the H_2 vibrational distribution following photodissociation of H_2CO.[1,4] Another proposal was put forward by Morokuma and co-workers, who reported roaming pathways to the NO+O_2 product from the ground and first excited electronic states, D_0 and D_1.[14] In the first report, a systematic reaction path search using CASPT2 calculations located a loose saddle point that connected the NO_3 minimum with the NO+O_2 products on D_0. The dynamics on D_1 is especially rich since dissociation to NO+O_2 can occur directly on that PES or a nonadiabatic transition, via a D_1/D_0 conical intersection, can occur to D_0, where these products can also form. Direct DFT trajectory calculations from the dissociation TS on the D_1 state gave vibrationally colder O_2, while those from the dissociation TS on the D_0 state gave vibrationally hotter O_2. However, these limited direct-dynamics calculations did not yield an O_2 vibration nearly as hot as experiment, which peaks at roughly v = 7. Nevertheless, this proposal of the two distinct channels explained North's experimental results and provided the first example of possible roaming dynamics that occurs on an excited electronic state. Subsequently, in a much more thorough analysis of the D_1 and D_0 PESs, three loose/"roaming" saddle points were located on the D_0 and D_1 PESs.[15]

Received: November 8, 2012
Published: December 18, 2012

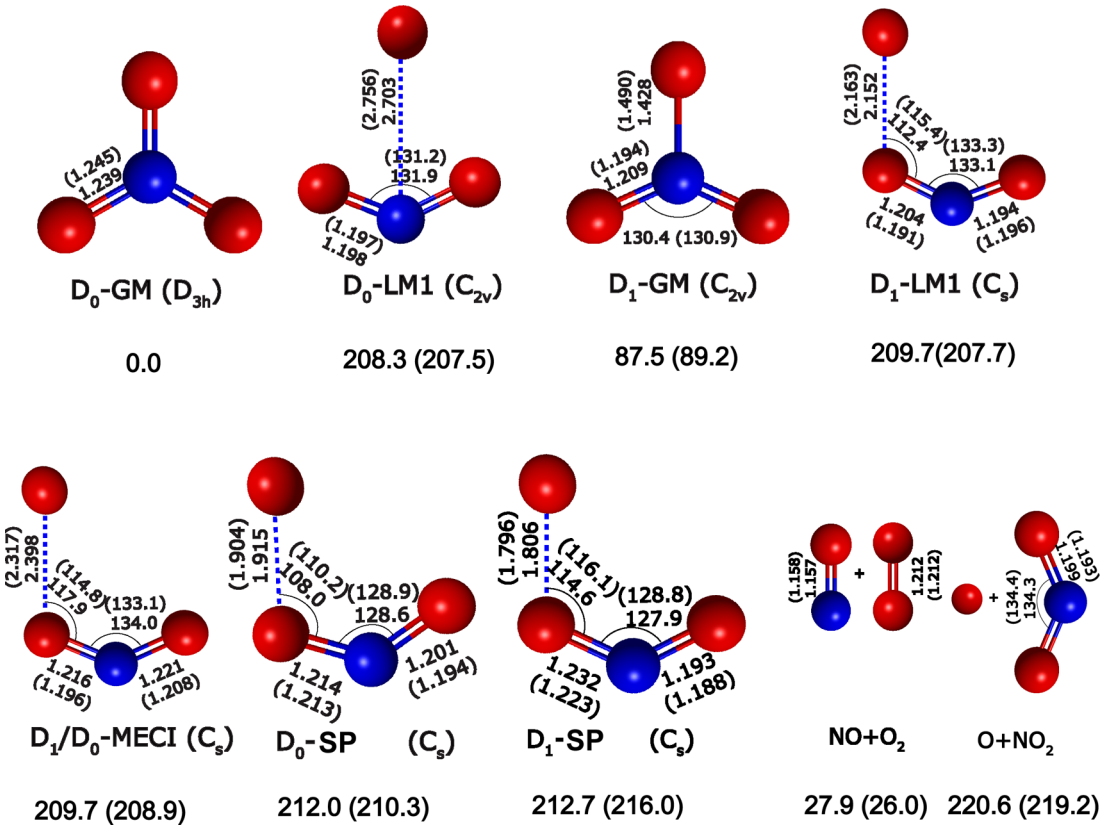

Figure 1. Optimized geometries (bond lengths in Å, angles in degree) and energies (kJ/mol) of the stationary points on the fitted PESs (in parentheses), compared with the results from the MS-CASPT2 calculations. The results for the D_0-SP and D_1-SP are compared between the current PESs (in parentheses) and previous PESs.[15]

In subsequent joint experimental and theoretical work, it was demonstrated that the photolysis of NO_3 to $NO+O_2$ proceeds exclusively via roaming pathways in both ground- and excited-state corresponding to the previously documented two distinct pathways, respectively.[16] North and co-workers further explored the stereodynamics of multistate roaming in the photolysis of NO_3 to NO + O_2 products.[17]

It is generally known that the roaming dynamics occur in a flat region of potential energy surface (PES), where nascent fragments move almost independently of each other and are able to sample many different relative orientations before an internal abstraction leading them to the final products. Since the roaming pathway bypasses the conventional tight transition state (TS), if one exists, the reaction products and kinetics in this unusual pathway cannot be predicted by standard transition state theory. Dynamics calculations on a global PES have proven to be an effective way to predict the fraction of roaming pathway and the corresponding properties of the products.[4,5] Up to now, the theoretical conclusions on the NO_3 roaming dynamics were derived from the PES characteristics and limited direct dynamics starting from the dissociation TS. It is essential then to perform dynamics calculations on global PESs to further investigate the roaming mechanisms in the photolysis of NO_3.

In this paper we report such calculations, specifically quasiclassical trajectory (QCT) calculations, on new *ab initio* PESs of the D_0 and D_1 states (FBXMM PESs), respectively. These are updated PESs based on the recently reported ones.[15] The detailed properties of the new D_0 and D_1 PESs, and the final products information, i.e., vibrational state, rotational state, and translational energy distributions of O_2 and NO products coming from the two surfaces, are presented and compared.

This paper is organized as follows. In section 2, we present the details for the construction of the new PESs and compare the relevant characteristics of the PESs to the high-level *ab initio* calculations. Section 3 gives the detailed QCT calculations and the results on D_0 and D_1 PESs. These include rovibrational state and translational energy distributions of O_2 and NO products from the D_0 and D_1 states, respectively. Comparisons of current QCT results and experimental results are made when possible. In section 4, we give the summary and conclusions.

2. POTENTIAL ENERGY SURFACES OF D_0 AND D_1 STATES

Full dimensional *ab initio* PESs for low-lying doublet states of NO_3 were reported recently by three of the co-authors (XMM) in this study.[15] However, dynamics studies, e.g., QCT or quantum dynamics calculations, on these PESs were not carried out and presented in that work. We initially performed QCT calculations on the D_0 and D_1 XMM PESs and found that the asymptotic regions of products O_2+NO and O+NO_2 were not properly described on them. Therefore, we added about 16 000 more *ab initio* data points to the original, roughly 74 000, data points of XMM PESs and fitted the new PESs to describe the regions of O_2+NO and O+NO_2 asymptotes and regions connecting roaming saddle points and O_2+NO products (postroaming regions). The electronic structure calculations for about 9000 data points in the postroaming regions were carried out by the multistate (MS)-CAS(17e,13o)PT2/aug-cc-pVTZ method using Molcas 7.4 and 7.6 programs,[18] which is the

dx.doi.org/10.1021/ct3009792 | J. Chem. Theory Comput. 2013, 9, 893−900

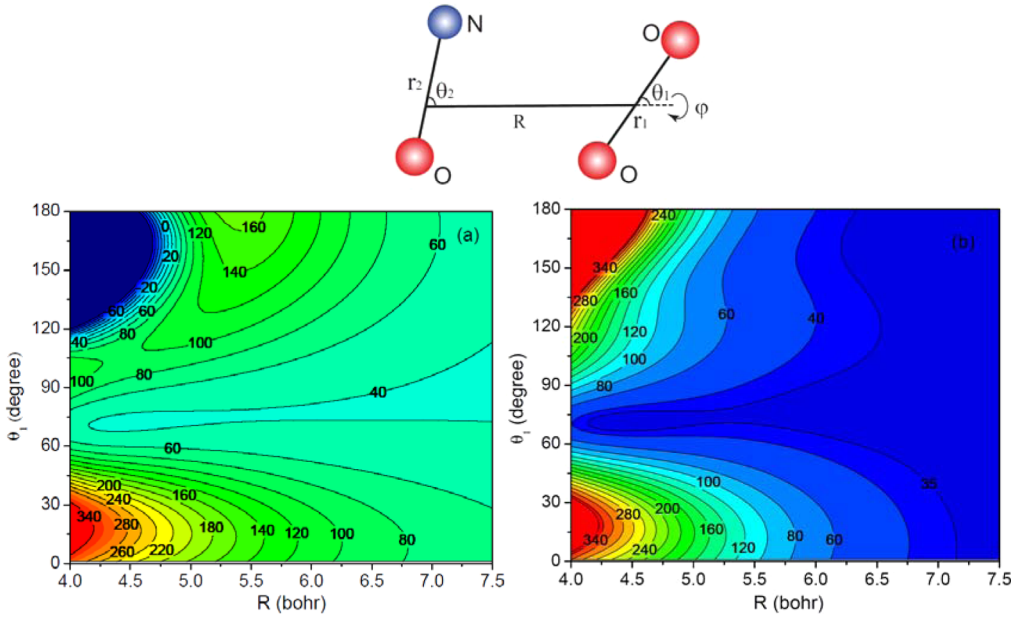

Figure 2. Contour plots of the old PES (a) and new PES (b) of D_0 state as functions of R and θ_1 coordinates fixed in the planar geometry. The Jacobi coordinates used in the plots are shown on the top of the figure. The other degrees of freedom are fixed with r_1 = 2.5 bohr, r_2 = 2.17 bohr, θ_2 = 65.0°.

same procedure as used in constructing the XMM PESs. The three-state averaging was employed with equal weight for the first three doublet states (D_0, D_1, and D_2) in the reference CASSCF calculations. The shift parameter 0.3 was applied in the CASPT2 calculations to avoid the intruder state problem. These configurations were mainly sampled by running quasi-classical dynamics calculations using preliminary PESs. Those trajectories were run from the roaming saddle point on the D_0 state, for the fixed total energies of 239 kJ/mol (the sum of experimental photolysis energy of 588 nm and zero-point energy (ZPE) of NO_3 global minimum of D_0) and microcanonical sampling of the initial momenta with total angular momentum J = 0. The energies of fragment data of O_2+NO and O+NO_2, for which the distances between center of masses of O_2 and NO and between O and NO_2 are larger than 9.0 bohr, were calculated by separating the fragments and assigning the energy as the sum of the fragment energies. The energies of fragments O_2, NO, and NO_2 were computed with RCCSD(T)/VTZ level of theory and basis by MOLPRO program.[19] The fragment data set consists of roughly 6000 data points for O_2+NO and 700 data points for O + NO_2 decomposition channels, respectively. Those energies were also shifted by roughly 14.5 kJ/mol for O_2+NO and 15.7 kJ/mol for O+NO_2 to be compatible with (MS)-CAS(17e,13o)PT2/aug-cc-pVTZ energies before being added to the large (MS)-CAS(17e,13o)PT2/aug-cc-pVTZ data set. Finally, a total of roughly 90 000 data points were included, respectively, for the new fits of D_0 and D_1 states. The PESs were fitted by basis of permutationally invariant polynomials of Morse-like variables in all internuclear distances [$y_{ij} = \exp(-r_{ij}/\lambda)$; where λ = 2.0 bohr]. Polynomials up to total order seven were used, for a total of 196 coefficients, for the D_0 and D_1 PESs, respectively. The fitting uses procedures developed in our group and recently reviewed.[20,21] These linear coefficients were obtained by standard linear least-squares fitting to all the data. The weighted RMS errors of the fitted D_0 and D_1 surfaces are 2.39 and 2.59 kJ/mol for energies up to 370 kJ/mol relative to the global minimum of D_0 PES, respectively.

A comparison of the geometries and energies of the global minima (GM), local minima (LM), and an Minimum-Energy Conical Intersection (MECI) for the ground and the first excited doublet states (D_0-GM, D_1-GM, D_0-LM, D_1-LM, D_1/D_0-MECI) from the fitted potential functions and directly from the *ab initio* MS-CASPT2 calculations is given in Figure 1. The NO-(r_e)+O_2(r_e) and O+NO_2(r_e) asymptotes, where "r_e" denotes to the equilibrium geometry, are also compared from the fitted PESs and direct *ab initio* calculations, which are single point calculations at the CAS(17e,13o)PT2/AVTZ level using separately optimized NO_2, NO, and O_2 fragments at the 3S-CAS(17e,12o)PT2/AVTZ, 3S-CAS(11e,8o)PT2/AVTZ, and 9S-CAS(12e,8o)PT2/AVTZ levels, respectively. As seen from the figure, the PESs describe the stationary points with good accuracy, with the maximum deviation of bond length from MS-CASPT2 results of 3%, bond angle of 3%, and energy of 2%. The NO(r_e)+O_2(r_e) and O+NO_2(r_e) channels on the fitted PESs are 26.0 and 219.2 kJ/mol relative to D_0-GM, respectively, which are very close to the *ab initio* values. Furthermore, the saddle points of O_2+NO channel on the D_0 and D_1 PESs, around which the abstraction of oxygen atom occurs, are important to the dynamics calculations, and thus we also show the structures and energies of D_0 saddle point (D_0-SP) and D_1-SP optimized on the fitted PESs in Figure 1. The O−O distance between the recombining oxygen atoms at D_0-SP is 1.903 Å, which is longer than the one at D_1-SP of 1.798 Å. These are quite close to the results of D_0-saddle3* and D_1-saddle3* obtained in the recent study.[15] The difference in the O−O distances has been identified previously as the apparent cause of the different vibrational excitation in the O_2 products produced on the different PESs. To some extent this is true; however, the present work indicates that post saddle-point regions of the PES, certainly for D_0, are very important to obtain vibrationally excited O_2.

Note that we added roughly 9000 data points in the postroaming regions and iterating between dynamics calculations and additional energies, to finally have the current PESs which are well converged respect to the dynamics results. Contour plots of the D_0 PES are shown as functions of R and θ_1

dx.doi.org/10.1021/ct3009792 | J. Chem. Theory Comput. 2013, 9, 893−900

(with other degrees of freedom fixed), in Figure 2(a) and Figure 2(b), respectively, for the preliminary PES fitted by about 81 000 combined data points of previous 74 000 MS-CASPT2/AVTZ[15] and current 7000 RCCSD(T)/AVTZ fragment energies, and the converged PES fitted by adding 9000 more data points in the postroaming regions based on the preliminary PES. The latter 9000 data points in the postroaming regions are essential, as the present PES gives the high vibrationally excitations of O_2 products on D_0 (see section 3), but the preliminary one did not. As seen from the two plots, the present PES is improved significantly compared with the preliminary one in the postroaming region, especially with the variation of the angle. It is very smooth with respect to the R and θ_1 coordinates.

3. QUASICLASSICAL TRAJECTORY CALCULATIONS

Standard quasi-classical trajectory (QCT) calculations were run on the new D_0 and D_1 PESs and were initiated at four different stating points: the D_0-GM, D_0-SP, D_1-GM, and D_1-SP. Trajectories were run at the total energy of 239 kJ/mol above D_0-GM, which corresponds to the photolysis energy of 588 nm when ZPE of D_0-GM is included. The excess energy was distributed to the Cartesian momenta in all degrees of freedom via random microcanonical sampling,[22] subject to the constraint of zero total angular momentum ($J = 0$). The trajectories were propagated with the time step of 0.12 fs using the velocity-Verlet integrator. Most of the trajectories starting from the saddle points were propagated for a maximum of 50 000 time-steps (~6 ps), indicating fairly prompt, direct dynamics from D_0-SP and D_1-SP to NO+O_2. In contrast, the maximum number of time-steps of trajectories initiated from D_0-GM and D_1-GM are 2 000 000 (~240 ps), implying that they stay at NO_3 complex for quite a long time and then dissociate via the roaming pathways (see below). The trajectories were terminated when one of the internuclear distances became larger than 14 bohr. Note that the other channel, O+NO_2, is also accessible at the total energy of 239 kJ/mol, and more than 99% of the trajectories go to this because of the direct dissociation pathway for this channel. As a result, a total of about 2 400 000 trajectories were run from D_0-GM, and only roughly 18 000 of them dissociated into O_2+NO products. The calculated results from D_1 are essentially independent of the initial configuration. We ran roughly 380 000 trajectories from D_1-GM (but only about 1300 of them result in O_2+NO), and thus the statistically more robust results from D_1-SP are shown below. A total of 150 000 trajectories were run from the saddle points of D_0 and D_1, respectively, and half of them dissociated into O_2+NO channel. We found most of the trajectories ended up dissociating into NO+O_2 or O+NO_2 using the maximum propagation time we set. For those trajectories from the global minima, we found all the O_2+NO products come from the roaming pathways on the D_0 and D_1 states. Two animations of roaming trajectories on D_0 and D_1 PESs are shown in the Supporting Information. They are characterized by incipient formation of O+NO_2, which, however, do not have enough energy to dissociate but instead orbit each other followed by oxygen atom self-abstraction to form O_2+NO. They also show that the O_2 product from D_0 is highly vibrationally excited, while that from D_1 is vibrationally cold. Figure 3 shows the dependence of potential energies on the propagation time for the two typical trajectories on D_0 and D_1 PESs, respectively. The NO_3 molecule first vibrates around the complex region, followed by the stretching out of one of N−O bonds. Then the roaming trajectories visit large flat regions of the PES, where the NO_3 complex nearly dissociates into O+NO_2, followed by the

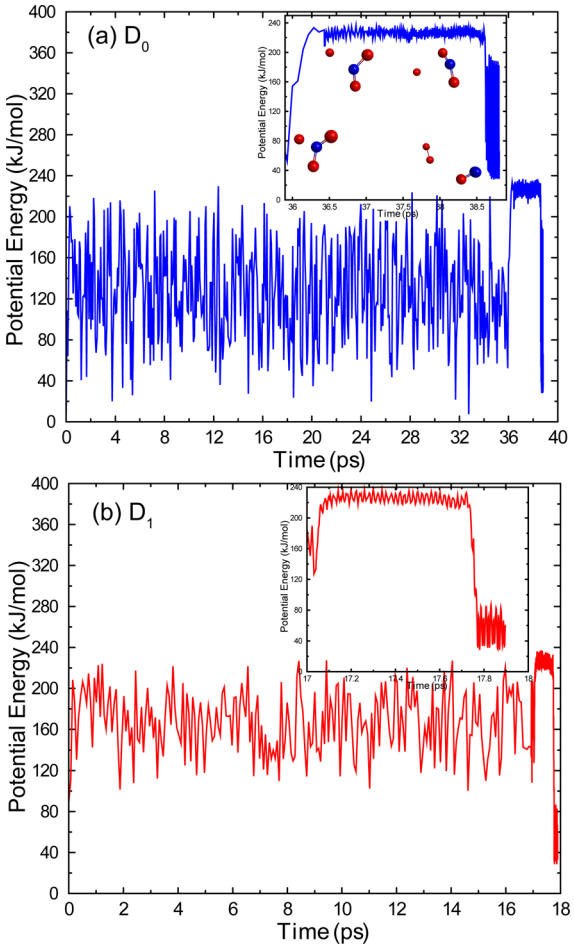

Figure 3. The potential energies relative to D_0-GM (kJ/mol) for the two sample roaming trajectories on D_0 (a) and D_1 (b) PESs as functions of time (fs). Insets show the flat potential of the roaming regions.

abstraction of oxygen atom. There is a minimum energy path on each surface connecting the region just after the initial N−O bond dissociation and the D_0- or D_1-SP region on the fitted PESs, as reported in the previous study.[15] Interestingly, many trajectories deviate significantly from such minimum energy paths, and also from other roaming saddle points (D_0-saddle1*, D_0-saddle2*, D_1-saddle1*, and D_1-saddle2*) located in the previous study.[15] This is not surprising, given the very flat nature of the PES in the roaming region. As the final state distributions were quite similar when considering different ZPE constraints, i.e., hard ZPE (each of the products has at least the corresponding ZPE), soft ZPE (the sum of the vibrational energies of products is not less than the sum of the corresponding ZPEs), and no ZPE, we show the statistically more robust results with no ZPE as follows.

The calculated vibrational distributions of O_2 for different rotational states of NO ($v = 0$, j_{NO}) on D_0 PES are shown in Figure 4. The results for trajectories initiated from D_0-GM and D_0-SP are displayed. Overall, the two batches of trajectories give rise to the similar O_2 vibrational distributions, showing that the O_2 product is highly vibrationally excited on D_0, with O_2 vibrational states that distribute up to $v = 11$. For low rotational states of NO (j_{NO} around 7), the vibrational distributions of O_2 are peaked at $v = 7$, which is in good agreement with North and co-workers' experiments.[13,16] With the increase of j_{NO}, the O_2 vibrations shift to lower states, as seen from the results for j_{NO}

dx.doi.org/10.1021/ct3009792 | J. Chem. Theory Comput. 2013, 9, 893−900

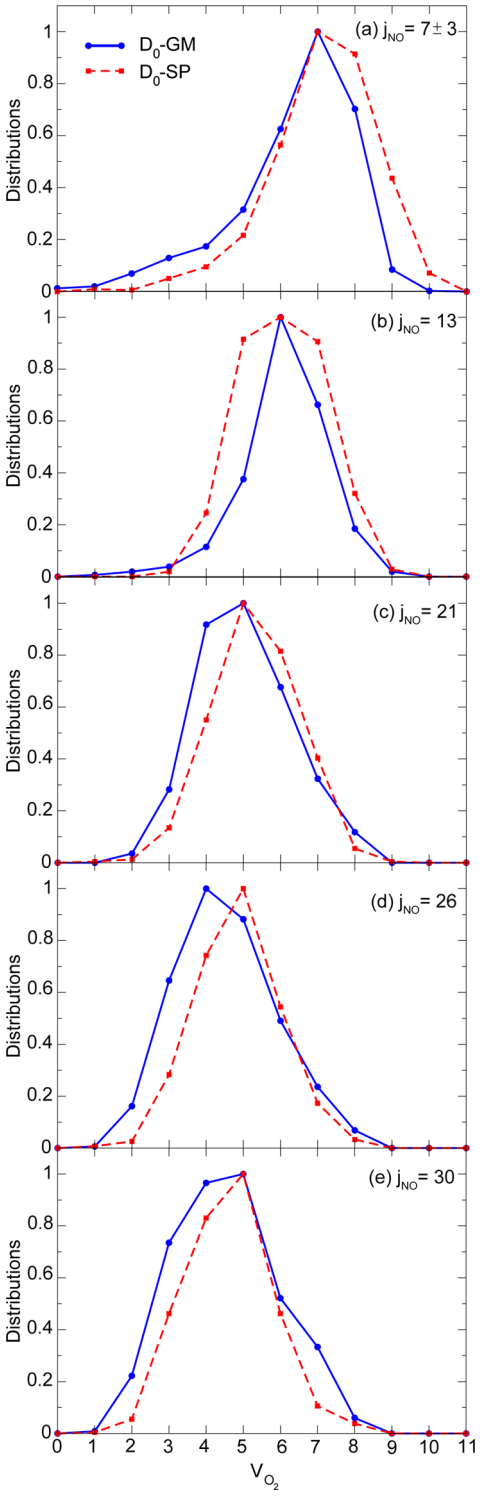

Figure 4. Vibrational state distributions of O_2 from the D_0 state for different regions of NO rotational states, NO (v = 0, j_{NO}).

varying from 13 to 30. The peak of vibrational distributions of O_2 shifts to v = 5 for higher j_{NO}. This decreasing O_2 vibrational excitation with the increase of j_{NO} is in agreement with experiment although the change is not as dramatic. For the high NO rotational states the partitioning between O_2 vibrational and rotational excitations is less certain from the experimental measurements and simulations, and thus for the highest rotational states individual vibrational contributions are unresolved.[13] Experimental results for the bimolecular reaction O + NO_2 show the O_2 vibrational distribution has a maximum at v = 6 in the range of 6 to 11, with no data reported for v < 6, as the absolute oscillator strengths for the $(0, v)$ bands vary quite widely and become so small for v < 6 that LIF signals are difficult to observe.[23] The present results are consistent with these earlier experiments.

Figure 5 shows O_2 vibrational distributions according to different NO (v = 0, j_{NO}) states on D_1 PES. In contrast to the

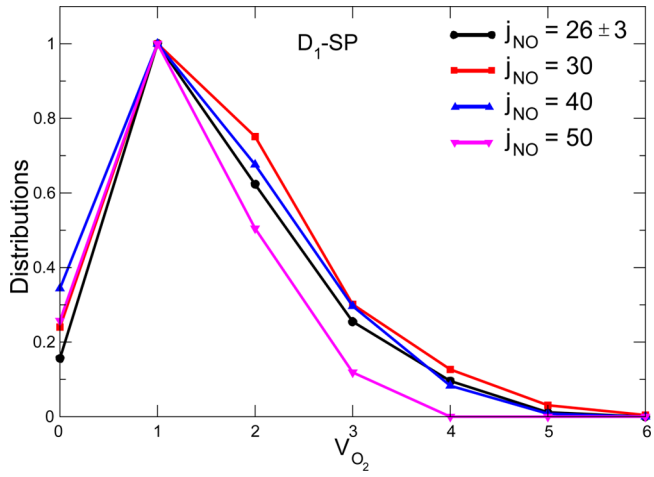

Figure 5. Vibrational state distributions of O_2 from the D_1 state for different regions of NO rotational states, NO (v = 0, j_{NO}).

results on D_0, O_2 is vibrationally cold on D_1, with the vibrational state that peaks at v = 1 and distributed up to v = 6. They exhibit no strong dependence on j_{NO}, which is in accordance with the experiment.[13] The different behavior of O_2 vibrational distributions both from roaming pathways on D_0 and D_1 states in the current dynamics study is in complete accord with the experimental and previous theoretical results and supposition that O_2 is formed vibrationally hot on D_0 but vibrationally cold on D_1.

The rotational distributions of O_2 on D_0 and D_1 states are presented in Figure 6. Here we do see differences, for the trajectories initiated from D_0-GM and D_0-SP, which is not the same case for the vibrational distributions. The distribution of j_{O2} from D_0-GM is quite broad, with the rotational states that distributed from j_{O2} = 0 to j_{O2} = 70 and peaked at around j_{O2} = 40. The distribution curve rises quickly to j_{O2} = 10, then slowly rises

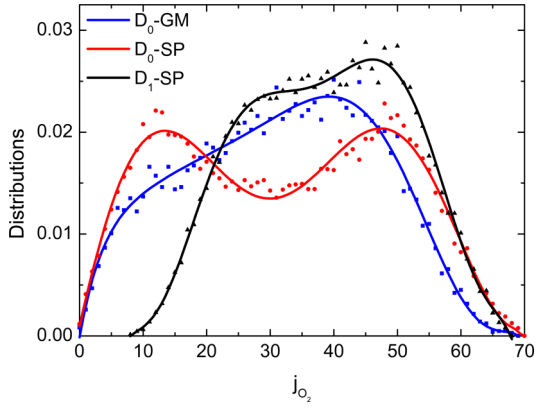

Figure 6. Total rotational state distributions of O_2.

dx.doi.org/10.1021/ct3009792 | J. Chem. Theory Comput. 2013, 9, 893−900

to the peak of j_{O2} = 40, and finally drops when j_{O2} increases further. In contrast, the O_2 rotational distribution from D_0-SP exhibits a bimodal distribution. We expect that the D_0 dynamics starts after N−O bond dissociation on the D_1 surface and subsequent internal conversion in the roaming region. This is because in the potential well of NO_3 the two PESs do not cross. After the N−O bond dissociation, two PESs are nearly degenerate giving the minimum energy CI at D_1/D_0-MECI. The transition may take place anywhere in the roaming region, and thus trajectories initiated from D_0-GM may be more reliable than those from D_1/D_0-MECI as well as from D_0-SP. As seen from the same figure, the rotational distribution of O_2 on D_1 shows even higher rotational excitations than those from D_0. This distribution is peaked at around j_{O2} = 50 and covers a wide range of j_{O2} between 8 and 70.

The calculated NO vibration is very cold from D_0 or D_1, with about 90% in $v = 0$, and the rest in $v = 1$. Thus we only present the rotational distributions of NO next. Figure 7 shows NO rotational distributions coming from the D_0 and D_1 PESs. In contrast to the O_2 rotational distributions, no significant differences are seen between the results for two batches of trajectories, one from D_0-GM and the other from D_0-SP. The former results show the distribution peaks at around j_{NO} = 22, and the latter with peaking at around j_{NO} = 27. Both of them are distributed up to j_{NO} = 50, with slightly higher rotational excitations from D_0-SP than D_0-GM. Furthermore, we see much more rotational excitations on D_1 than D_0 in Figure 6; this distribution rises from j_{NO} = 15, peaks at j_{NO} around 35, and vanishes around j_{NO} = 60. The calculated NO rotational distributions are in good agreement with the experimental measurements.[13]

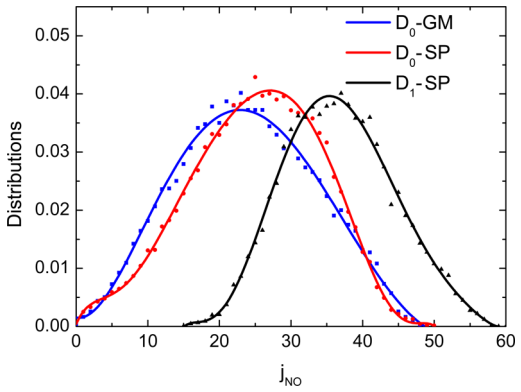

Figure 7. Total rotational state distributions of NO.

Next we consider the translational energy distributions of O_2+NO products. The translational energy distributions on D_0 for different regions of rotational states of NO (v = 0, j_{NO}) are shown in Figure 8. The results obtained from the trajectories initiated from D_0-GM are close to those from D_0-SP, with average deviations of roughly 10 kJ/mol. For small NO rotational states (j_{NO} in the range of [4, 10]), the translational energy distribution is peaked around 45 kJ/mol for D_0-GM, and 55 kJ/mol for D_0-SP, with the two distribution curves distributed up to 160 kJ/mol. As j_{NO} increases, the peak of translational energy distribution exhibits a slight shift to higher energy, but the distribution becomes more localized. These results agree well with the translational energy distribution of specific rotational states of NO from the experiment.[13] Note that for the high rotational states of NO, the experimental translational energy shows a bimodal distribution, which corresponds to the theoretically lower translational energies from D_0 and higher translational energies from D_1, respectively, with some overlap of both of them in the medium energy region.

The reaction on D_1 gives rise to higher translational energy than on D_0, as seen from Figure 9 for the translational energy distributions of O_2+NO for different regions of NO rotational states on D_1. The distributions rise from E_{trans} = 50 kJ/mol, peaking at around E_{trans} = 105 kJ/mol, and then drop gradually, with the maximum of translational energy at 160 kJ/mol, 155 kJ/

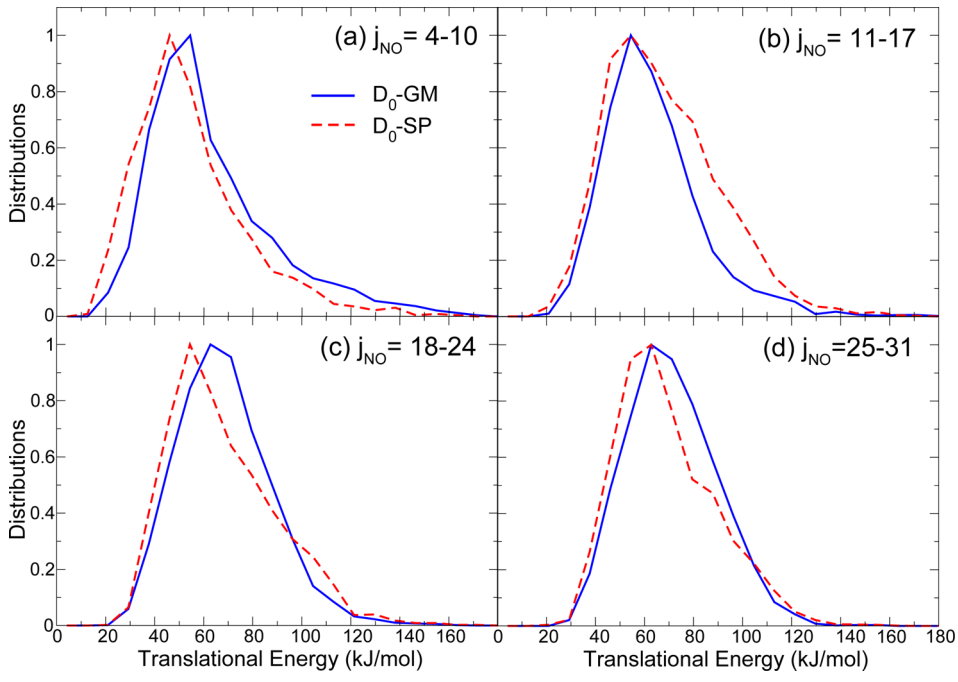

Figure 8. Translational energy distributions of NO+O_2 from the D_0 state, for different regions of NO rotational states.

dx.doi.org/10.1021/ct3009792 | J. Chem. Theory Comput. 2013, 9, 893−900

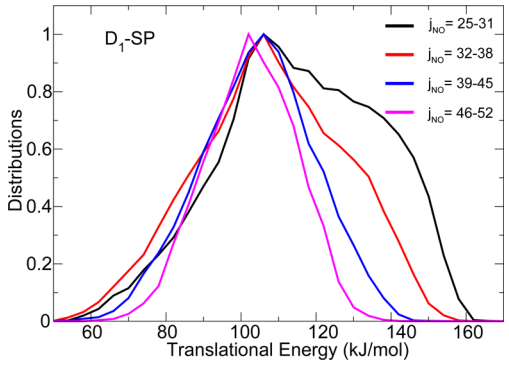

Figure 9. Translational energy distributions of $NO+O_2$ from the D_1 state, for different regions of NO rotational states.

mol, 145 kJ/mol, and 140 kJ/mol for j_{NO} in the range of [25, 31], [32, 38], [39, 45], and [46, 52], respectively.

To summarize thus far, the current QCT calculations on the new D_0 PES show the pathway which is characterized by vibrationally excited O_2, rotationally cold NO; while the reaction pathway on the D_1 PES produces vibrationally colder O_2 and rotationally hotter NO, which supports the experimental results that the dominant pathway with hot O_2 vibration and cold NO rotation is the roaming pathway on D_0 and the other one with cold O_2 vibration and hot NO rotation is the roaming on D_1. Furthermore, the theory clearly shows that more energy is released as translational motion on D_0 than that is on D_1. We also found the total internal energy distributions of O_2 peaking at around 120 kJ/mol, which is in very good agreement with Wittig's experiment showing the peak also around 120 kJ/mol.[24]

Finally, we briefly consider the **v**-**j** vector correlation of NO fragments. We show the distributions of angle between the velocity vector **v** and the angular momentum vector **j** (v-j angle) in Figure 10 (a) for the D_0 state and Figure 10(b) for the D_1 state, respectively. The distributions of v-j angle from D_0 and D_1 show a peak of around 90°, indicating strong perpendicular correlations between v and j in the NO fragment originating from both pathways, which is in agreement with the experimental measurements suggesting a constrained planar dissociation.[17] The predominantly planar dissociation on D_0 and D_1 is well verified in the QCT calculations by checking the dominance of the planarity of final products. These results were discussed in light of the absence of vector correlations in other roaming systems, which have previously been characterized by an unconstrained intramolecular abstraction.[1,5] It is interesting to see that geometrical constraints should actually be quite prevalent in roaming dynamics and are analogous to the geometrical constraints of the corresponding bimolecular abstraction reaction.

4. SUMMARY AND CONCLUSIONS

To summarize, new *ab initio* global PESs of ground (D_0) and the first excited (D_1) electronic states for photodissociation of NO_3 are calculated in this study. The PESs are constructed by fitting roughly 90 000 MS-CAS(17e,13o)PT2/aug-cc-pVTZ calculations of electronic energies, using permutationally invariant polynomials. The QCT calculations have been performed on the fitted PESs, and detailed dynamics information of $NO+O_2$ products for vibrational state, rotational state, translational energy distributions were presented and compared with the experimental results when possible. Good agreement between the QCT calculations and experiment has been achieved; the

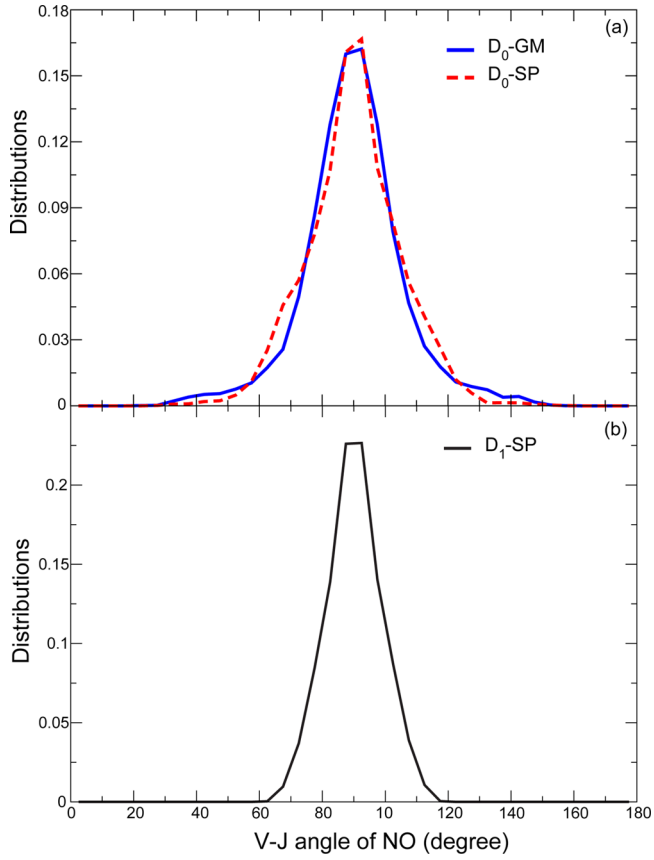

Figure 10. The distributions of the v-j angle of NO fragments (the angle between the velocity vector **v** and angular momentum vector **j**), from D_0 (a) and D_1 (b) states.

reaction on the D_0 state gives rise to vibrationally excited O_2 and rotationally cold NO, while the reaction on D_1 produces vibarationally colder O_2 and rotationally hot NO, with both reactions originating from the roaming pathways on the two states. This is the first dynamics study of NO_3 photodissociation which fully supports the proposal of roaming dynamics on the excited and ground states. Furthermore, differently from other roaming systems, the strong perpendicular correlation between **v** and **j** vectors of the NO fragment is obtained from the current calculations, which supports the experimental measurements too. A study of the two j_{O2}-j_{NO} vector correlations requires many more trajectories than we ran but that would be interesting and something we plan to do in the future. The work on bimolecular reaction of $O+NO_2 \rightarrow O_2+NO$ is underway and expected to be reported later. The comparison made with the recent experimental work of Mar et al.[25] will also be discussed.

■ ASSOCIATED CONTENT

Supporting Information

The two animations of roaming trajectories initiated from D_0-GM and D_1-GM, respectively. This material is available free of charge via the Internet at http://pubs.acs.org.

■ AUTHOR INFORMATION

Corresponding Author

*E-mail: bina@dicp.ac.cn.

Notes

The authors declare no competing financial interest.

■ ACKNOWLEDGMENTS

J.M.B. thanks the Army Research Office (W911NF-11-1-0477) for financial support. This work is partly supported by a grant from Japan Society for the Promotion of Science (Grants-in-Aid for Scientific Research <KAKENHI> No. 23685004) at Hokkaido University, as well as a grant from US AFOSR (Grant No. FA9550-10-1-0304) at Emory University. A majority of single point CASPT2 calculations were performed using the computational resources in Institute for Molecular Science, Okazaki, Japan.

■ REFERENCES

(1) Bowman, J. M.; Shepler, B. C. *Annu. Rev. Phys. Chem.* **2011**, *62*, 531−553.
(2) Suits, A. G. *Acc. Chem. Res.* **2008**, *41*, 873−881.
(3) Osborn, D. L. *Adv. Chem. Phys.* **2008**, *138*, 213−265.
(4) Townsend, D.; Lahankar, S.; Lee, S. K.; Chambreau, S. D.; Suits, A. G.; Zhang, X.; Rheinecker, J.; Harding, L. B.; Bowman, J. M. *Science* **2004**, *306*, 1158−1161.
(5) Houston, P. L.; Kable, S. H. *Proc. Natl. Acad. Sci. U.S.A.* **2006**, *103*, 16079−16082.
(6) Heazlewood, B. R.; Jordan, M. J. T.; Kable, S. H.; Selby, T. M.; Osborn, D. L.; Shepler, B. C.; Braams, B. J.; Bowman, J. M. *Proc. Natl. Acad. Sci. U.S.A.* **2008**, *105*, 12719−12724.
(7) Goncharov, V.; Herath, N.; Suits, A. G. *J. Phys. Chem. A* **2008**, *112*, 9423−9428.
(8) Harding, L. B.; Klippenstein, S. J. *J. Phys. Chem. Lett.* **2010**, *1*, 3016−3020.
(9) Hause, M. L.; Herath, N.; Zhu, R.; Lin, M. C.; Suits, A. G. *Nat. Chem.* **2011**, *3*, 932−937.
(10) Chen, C.; Braams, B. J.; Lee, D. Y.; Bowman, J. M.; Houston, P. L.; Stranges, D. *J. Phys. Chem. Lett.* **2010**, *1*, 1875−1880.
(11) Kamarchik, E.; Koziol, L.; Reisler, H.; Bowman, J. M.; Krylov, A. I. *J. Phys. Chem. Lett.* **2010**, *1*, 3058−3065.
(12) Grubb, M. P.; Warter, M. L.; Suits, A. G.; North, S. W. *J. Phys. Chem. Lett.* **2010**, *1*, 2455−2458.
(13) Grubb, M. P.; Warter, M. L.; Johnson, K. M.; North, S. W. *J. Phys. Chem. A* **2011**, *115*, 3218−3226.
(14) Xiao, H.; Maeda, S.; Morokuma, K. *J. Phys. Chem. Lett.* **2011**, *2*, 934−938.
(15) Xiao, H.; Maeda, S.; Morokuma, K. *J. Chem. Theory. Comput.* **2012**, *8*, 2600−2605.
(16) Grubb, M. P.; Warter, M. L.; Xiao, H.; Maeda, S.; Morokuma, K.; North, S. W. *Science* **2012**, *335*, 1075−1078.
(17) Grubb, M. P.; Warter, M. L.; North, S. W. *Phys. Chem. Chem. Phys.* **2012**, *14*, 6733−6740.
(18) Aquilante, F.; Vico, L.; De; Ferre, N.; Ghigo, G.; Malmqvist, P.-Å; Neogrady, P.; Pedersen, T. B.; Pitonak, M.; Reiher, M.; Roos, B. O.; Serrano-Andres, L.; Urban, M.; Veryazov, V.; Lindh, R. *J. Comput. Chem.* **2010**, *31*, 224−227.
(19) Werner, H.-J.; Knowles, P. J.; Lindh, R.; Manby, F. R.; Schütz, M.; Celani, P.; Korona, T.; Mitrushenkov, A.; Rauhut, G.; Adler T. B.; et al. *MOLPRO, A Package of Ab Initio Programs*, version 2010.1. http://www.molpro.net.
(20) Braams, B. J.; Bowman, J. M. *Int. Rev. Phys. Chem.* **2009**, *28*, 577−606.
(21) Bowman, J. M.; Czakó, G.; Fu, B. *Phys. Chem. Chem. Phys.* **2011**, *13*, 8094−8111.
(22) Hase, W. L. Classical Trajectory Simulations: Initial Conditions. In *Encyclopedia of Computational Chemistry*; Allinger, N. L., Ed.; Wiley: New York, 1998; Vol. *1*, pp 402−407.
(23) Smith, I. W. M.; Tuckett, R. P.; Whitham, C. J. *Chem. Phys. Lett.* **1992**, *200*, 615−623.
(24) Mikhaylichenko, K.; Riehn, C.; Valachovic, L.; Sanov, A.; Wittig, C. *J. Chem. Phys.* **1996**, *105*, 6807−6817.
(25) Mar, K. A.; Wyngarden, A. L. V.; Liang, C.-W.; Lee, Y. T.; Lin, J. J.; Boering, K. A. *J. Chem. Phys.* **2012**, *137*, 044302-1-12.